Journal of Biomolecular NMR
https://doi.org/10.1007/s10858-024-00436-9

ARTICLE

DNP-assisted solid-state NMR enables detection of proteins at nanomolar concentrations in fully protonated cellular milieu

Whitney N. Costello[1] · Yiling Xiao[1] · Frederic Mentink-Vigier[2] · Jaka Kragelj[1,4] · Kendra K. Frederick[1,3]

Received: 9 November 2023 / Accepted: 9 February 2024

Abstract

With the sensitivity enhancements conferred by dynamic nuclear polarization (DNP), magic angle spinning (MAS) solid state NMR spectroscopy experiments can attain the necessary sensitivity to detect very low concentrations of proteins. This potentially enables structural investigations of proteins at their endogenous levels in their biological contexts where their native stoichiometries with potential interactors is maintained. Yet, even with DNP, experiments are still sensitivity limited. Moreover, when an isotopically-enriched target protein is present at physiological levels, which typically range from low micromolar to nanomolar concentrations, the isotope content from the natural abundance isotopes in the cellular milieu can outnumber the isotope content of the target protein. Using isotopically enriched yeast prion protein, Sup35NM, diluted into natural abundance yeast lysates, we optimized sample composition. We found that modest cryoprotectant concentrations and fully protonated environments support efficient DNP. We experimentally validated theoretical calculations of the limit of specificity for an isotopically enriched protein in natural abundance cellular milieu. We establish that, using pulse sequences that are selective for adjacent NMR-active nuclei, proteins can be specifically detected in cellular milieu at concentrations in the hundreds of nanomolar. Finally, we find that maintaining native stoichiometries of the protein of interest to the components of the cellular environment may be important for proteins that make specific interactions with cellular constituents.

Keywords DNP solid-state NMR · In-cell NMR · Sup35 · Yeast prions

Introduction

Biological processes occur in complex environments containing a myriad of potential interactors. In-cell NMR allows us to obtain atomic resolution information of proteins in their native environments (Selenko et al. 2006; Inomata et al. 2009; Sakakibara et al. 2009; Banci et al. 2013; Theillet et al. 2013; Freedberg and Selenko 2014; Burmann et al. 2020). Magic angle spinning (MAS) solid-state NMR is particularly useful to study proteins and their interactions inside cells (Gupta et al. 2016; Kaplan et al. 2016a, b; Qiang et al. 2017; Albert et al. 2018; Narasimhan et al. 2019a, b; Scherpelz et al. 2021). With the sensitivity gains conferred by dynamic nuclear polarization (DNP), MAS NMR has the sensitivity to detect proteins at very low concentrations in complex biological environments (Frederick et al. 2015; Albert et al. 2018; Costello et al. 2019; Narasimhan et al. 2019a, b; Bertarello et al. 2022). This opens up the possibility of investigation of proteins at their native contexts and with their native stoichiometries relative to potential interactors. While the endogenous concentration of some abundant proteins can exceed a hundred micromolar (Nollen and Morimoto 2002), most proteins are present at concentrations between 10 nM and 10 µM in yeast cells and between 1 nM and 1 µM in cultured mammalian cells (Wang et al. 2012). With the development of both the instrumentation and polarization agents for DNP continually improving the sensitivity of DNP NMR, detection of more and more proteins at their endogenous concentrations, where native stoichiometries are maintained, will potentially become possible.

✉ Kendra K. Frederick
kendra.frederick@utsouthwestern.edu

1 Department of Biophysics, UT Southwestern Medical Center, Dallas, TX 75390-8816, USA

2 National High Magnetic Field Lab, Florida State University, Tallahassee, FL, USA

3 Center for Alzheimer's and Neurodegenerative Disease, UT Southwestern Medical Center, Dallas, TX 75390, USA

4 Present Address: Slovenian NMR centre, National Institute of Chemistry, Hajdrihova 19, 1000 Ljubljana, Slovenia

Published online: 23 March 2024

The effectiveness of DNP-enhanced MAS NMR is critically dependent on sample composition and experimental conditions. Early biological DNP NMR investigations were optimized on purified samples at high concentrations (Hall et al. 1997; van der Wel et al. 2006). Because DNP NMR experiments are typically performed at low temperatures, biological samples are cryoprotected to avoid ice crystal formation and ensure homogenous dispersion of the polarization agent throughout the sample. In early work, samples of biomolecules were often cryoprotected by adding 60% d_8-glycerol (*v*/*v*), because much of the early biological DNP work was on the light-sensitive protein bacteriorhodopsin (Rosay et al. 2001, 2003; Bajaj et al. 2007) and 60:40 glycerol:water mixtures form optically-clear glasses at all freezing rates (Lane 1925; Inaba and Andersson 2007). Moreover, because polarization transfer from the early generation of polarization agents like TEMPO (Bajaj et al. 2003) and TOTAPOL (Song et al. 2006) was most efficient in per-deuterated settings, the DNP matrix was optimized to have a buffer protonation level of 10% (*v*/*v*).(Rosay 2001). Even though many different matrix compositions can support glass formation (Tran et al. 2020) and polarization transfer mechanisms from the newer generation of polarization agents do not necessarily require sample per-deuteration (Lund et al. 2020; Harrabi et al. 2022), the matrix composition of 60:30:10 d_8-glycerol:D_2O:H_2O, which is often referred to as "DNP juice", remains widely and successfully used for DNP NMR investigations of purified biological molecules (Heiliger et al. 2020; Zhai et al. 2020; Elathram et al. 2022).

Despite broad usage, DNP juice may not support the highest possible experimental sensitivity, particularly for heterogenous samples. With the 60:30:10 composition, most of the volume of the sample is made up of glycerol, which decreases the rotor fill factor. Moreover, high per-deuteration reduces the number of protons at exchangeable sites and decreases absolute sensitivity. For example, optimization of the lipids and the type of cryoprotectant used for DNP NMR of membrane protein samples doubled DNP efficiency (Liao et al. 2016). Likewise, modern polarization agents generate faster polarization transfer, via stronger electron–electron couplings (Mentink-Vigier et al. 2017) and are thus less sensitive to the protonation level of the matrix (Harrabi et al. 2022). Because cellular milieu has different glassing properties than concentrated samples of purified isolated proteins, high concentrations of cryoprotectants may not be necessary. Doing so would increase the rotor fill factor and dramatically increase experimental sensitivity. Moreover, because cellular systems do not always tolerate deuteration well (Misra 1967), avoiding per-deuteration may not only increase the experimental sensitivity at exchangeable sites but also better maintain the biology integrity of the sample. Thus, modifying the composition of the DNP matrix for multi-component samples can potentially dramatically increase experimental sensitivity beyond the current state of the art and because these experiments are sensitivity limited it is important to do so.

Finally, most samples for modern biological NMR are isotopically enriched and when a sample contains a mixture of isotopically enriched and un-enriched sites, the contribution of the signal from natural abundance isotopes (at 1.1% of carbons and 0.37% of nitrogen) to the NMR spectra can typically be ignored (Schubeis et al. 2015; Gupta and Tycko 2018). While the sensitivity enhancements conferred by DNP are theoretically sufficient to enable detection of proteins at their endogenous concentrations (van der Zwan et al. 2021), the increase in experimental sensitivity conferred by DNP is also sufficient to enable the study of biomolecules containing only naturally abundant NMR active isotopes (Takahashi et al. 2012; Mollica et al. 2015; Märker et al. 2017; Kang et al. 2019). Thus, for samples of an isotopically labeled protein present at its endogenous concentration in concentrated cellular milieu, it is possible, and even likely, that the number of NMR active isotopes present in the sample due to natural abundance will outnumber those in the isotopically enriched protein. Most solid state NMR studies of isotopically enriched proteins in native biological settings have focused on proteins present at concentrations in the high tens to hundreds of micromolar, where contributions from the natural abundance proteins in the biological setting have not been problematic (Renault et al. 2012; Kaplan et al. 2016a, b; Narasimhan et al. 2019a, b). A study of the yeast prion protein, Sup35NM, at endogenous levels in a biological setting at a concentration of 1 μM used isotopically depleted cellular milieu to eliminate the signals from natural abundance components that otherwise contributed to the spectra (Frederick et al. 2015). However, with the improvements in both instrumentation (Berruyer et al. 2020) and development of more efficient polarization agents (Sauvee et al. 2013; Harrabi et al. 2022), the characterization of proteins at even lower concentrations is experimentally tractable. Knowing the analyte concentrations that can theoretically be specifically detected over the natural abundance molecules in the sample is critical for interpretation.

In the study of Sup35NM, structural changes occurred in a region of the protein that is known to influence biological activity but is intrinsically disordered in purified samples. In that study, isotopically enriched Sup35NM was added to yeast lysates at endogenous levels, maintaining native stoichiometries with potential interactors. (Frederick et al. 2015) Maintaining the relative stoichiometries of Sup35 to the chaperones proteins is critical to retain inheritance of this functional prion from mother to daughter cell (Allen et al. 2005; Masison et al. 2009; Helsen and Glover 2012; Kiktev et al. 2012). However, it is unclear if maintaining the native stoichiometry of the protein of interest to the components

of the cellular environment is an important experimental consideration. Uncertainty about this point complicates interpretation of the data of in-cell experiments, limiting the utility of that information. Here, we work with Sup35NM system because yeast tolerate growth in per-deuterated environments. Moreover, working in minimally diluted pelleted lysed cells—the final macromolecular concentration in these samples is lower than that in intact cells by about a third—enables control over sample composition. Finally, prior work in this system revealed that a region of Sup35NM that is disordered in purified settings becomes structured when the protein is investigated at its endogenous levels in biological settings (Frederick et al. 2015; Costello et al. 2019). To optimize the composition of the DNP matrix to maximize sensitivity, we altered the cryoprotectant content and amount of per-deuteration the DNP matrix and cellular milieu. To determine the limits of specificity in systems of isotopically enriched proteins in concentrated mixtures of biological molecules we validate theoretical calculations with experimental measurements. Working at a concentration of 25 µM Sup35NM that is an order of magnitude over the endogenous level, we examine the effect of altering native stoichiometries on a protein whose structure is influenced by biological environments.

Results

Moderate concentrations of glycerol result in the best DNP performance

Because the DNP enhancements that increase experimental sensitivity depend on sample composition, we assessed DNP performance of samples of proteins diluted in yeast lysates made with different amounts of cryoprotectant as well as different deuteration levels of both the buffer and the components of the cellular lysates. To determine the optimal amount of cryoprotectant for proteins at low concentrations in cellular lysates, we prepared samples with different amounts of the cryoprotectant glycerol and measured the DNP enhancements using a uniform recycle delay of 4 s. We also determined the absolute signal intensity for the protein component. To do so, we collected ^{15}N-filtered zTEDOR spectra which select for adjacent ^{13}C–^{15}N pairs which are over-represented in the added Sup35NM protein (Jaroniec et al. 2002). Samples containing 15% glycerol (*v*/*v*) had the highest sensitivity. Using a uniform recycle delay of 7 s, DNP enhancements for lysate samples prepared without any cryoprotection were 30 ± 10% smaller while the DNP enhancements of samples that contained 60% glycerol were 50 ± 10% smaller than the DNP enhancements of samples that contained 15% glycerol (Fig. 1B, black). The absolute signal intensity for Sup35NM, as determined by ^{15}N-filtered

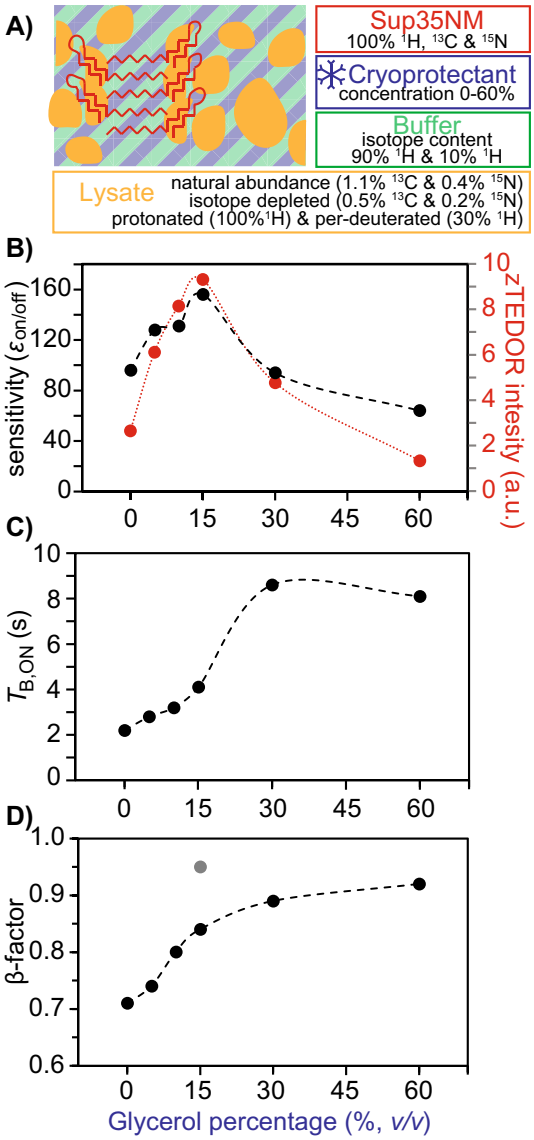

Fig. 1 Lower cryoprotectant percentages result in better DNP performance of dilute proteins in pelleted cellular lysates. **A** Sup35NM (red) is diluted in a matrix composed of cryoprotectant (blue), solvent in the buffer (green) and cellular components (yellow), all of which can have different concentrations and isotope content. **B** DNP enhancement collected with a recycle delay of 7 s, $\varepsilon_{on/off}$ (black) and raw signal intensity from Sup35NM (red) using zTEDOR (^{15}N-^{13}C) of the carbonyl peak are both dependent upon the percentage of glycerol in the sample. **C** The build-up time values, $T_{B,ON}$, derived from ^{1}H-saturation recovery experiments fit to a stretched exponential function at the carbonyl are dependent upon the percentage of glycerol in the sample. **D** The β-factor from the ^{1}H-saturation recovery experiments fit to stretched exponential decrease upon the percentage of glycerol for pelleted lysates (black) and complete lysates (gray). Samples in perdeuterated natural abundance lysates and buffer with 10% H_2O. Dotted lines are to guide the eye. Data from one out of three independent sets of samples are shown

zTEDOR spectra, also occurs at 15% glycerol (Fig. 1B, red). Because the recycle delay was shorter than the build-up time for some samples, we calculated the DNP enhancement for a uniform recycle delay of 1.3 times the build up time and found that the calculated DNP enhancements increased until samples contained 15% glycerol and then were similar for samples with higher glycerol concentrations. In contrast, the calculated spectral intensities for the ^{15}N-filtered zTEDOR spectra were similar to the reported value because the difference in fill factor altered the absolute sensitivity. Thus, cryoprotection with 15% glycerol resulted in the best DNP performance.

We next determined build up times ($T_{B,ON}$) of the yeast lysate components by fitting the carbonyl carbon (~ 175 ppm) in the ^{13}C–CP spectra to a stretched exponential function. If the concentration distribution of AMUPol is homogenous, the exponential will not be stretched, and β will equal 1. If the concentration distribution of AMUPol is heterogenous, there will be a mixture of underlying $T_{B,ON}$ values, the increase in the range of $T_{B,ON}$ values are best fit with more stretch and the value of β decreases (Rankin et al. 2019; Pinon et al. 2017) (Fig. 1C). Although these samples all contained similar amounts of AMUPol, the $T_{B,ON}$ increased with cryoprotectant concentration from 2 s for samples without glycerol to 8 s for samples containing 60% glycerol (Fig. 1C). Interestingly, the β-factor also increased from 0.75 for samples without glycerol to 0.93 for samples containing 60% glycerol (Fig. 1D). Glycerol improved the dispersion of the radical throughout this complicated system; the covariance of $T_{B,ON}$ with β-factor suggested that the short $T_{B,ON}$ values for samples with smaller amounts of glycerol results from inhomogeneous dispersion of the radical in these sample. However low cryoprotectant percentage are not responsible for short values of $T_{B,ON}$ because the $T_{B,ON}$ of proline frozen with different amounts of glycerol did not show a decrease in the β-factor (β-factor = 0.97). This suggests that the change in $T_{B,ON}$ values in lysate samples results from inhomogeneous dispersion of the radical and that glycerol improved the dispersion of the radical throughout this complicated system although at the expense of sensitivity and $T_{B,ON}$. To determine if inhomogenous radical dispersion was a general property of cellular milieu or if it was a result of the lysate sample preparation, we prepared cellular lysates using an alternative method. We prepared lysates where the small molecule component of the sample was not removed by centrifugation before addition of 15% glycerol. We found that the fit of the build-up time for these lysates had a β-factor of 0.95, indicating that the inhomogeniety for the lysate samples resulted from the sample preparation (Fig. 1D, gray point) and is not a general property of radical dispersion in cellular milieu with low concentrations of cryoprotectants. Taken together, samples containing 15% glycerol or more had the highest enhancements and, because of the improved fill factor and shorter build up time, samples containing 15% glycerol had the highest overall sensitivity as well. Using 15% glycerol rather than 60% glycerol as a cryoprotectant doubles the experimental sensitivity (Fig. 1B, red).

AMUPol is a highly efficient, water soluble, commercially available polarization agent. While typically used in per-deuterated environments, efficient polarization transfer from AMUPol may not require per-deuteration, even at high fields. To assess this, we first determined the dependence of DNP enhancement and $T_{B,ON}$ on increasing protonation content for a standard sample of uniformly isotopically labeled proline in 60/40 glycerol/water mixtures (Figure S1). The DNP enhancement was highest when the sample contained 10% H_2O (*v/v*) and decreased by ~ 30% in a fully protonated setting while the $T_{B,ON}$ values were longer by a second ($p < 0.05$, student's t-test, n = 4) (Figure S1A). To determine if analyte concentration affected DNP performance, as assessed by the magnitude of the DNP enhancement and the $T_{B,ON}$ values, we varied the proline concentration by five orders of magnitude and measured DNP enhancements and $T_{B,ON}$ values. Neither the DNP enhancement or $T_{B,ON}$ value were sensitive to analyte concentration (Figure S1B). Thus, the DNP performance (DNP enhancement and $T_{B,ON}$ values) of AMUPol is modestly improved by high deuteration levels of the buffer.

Fully protonated environments support efficient DNP performance

Because per-deuteration is not always well tolerated by cellular systems (Misra 1967), we determined the DNP enhancement and $T_{B,ON}$ values for proteins at low concentrations in cellular lysates when AMUPol is used as a polarization agent with a variety of deuteration levels. To determine if per-deuteration of the cellular lysate is required for efficient polarization transfer from the polarization agent, AMUPol, to the isotopically labeled protein of interest in samples containing cellular lysates and cryoprotected with 15% glycerol, we varied both the protonation level of the DNP sample buffer as well as the cellular lysates. First, we tested the effect of DNP sample buffer protonation levels on DNP sample performance while holding the per-deuteration level of the cellular lysates constant. We tested DNP sample buffer protonation levels of 10% and 85%. To do so, we prepared three independent DNP NMR samples of deuterated cellular lysates with 25 µM uniformly ^{13}C, ^{15}N-labeled Sup35NM protein, 15% d_8-glycerol, 5 mM AMUPol biradical (Figure S2) and measured DNP enhancement and build up times (Fig. 2, right). We found the DNP enhancement did not change (Fig. 2A, right) but the build-up time for the sample containing 10% H_2O was several seconds shorter than it was for the sample containing 85% H_2O (Fig. 2B,

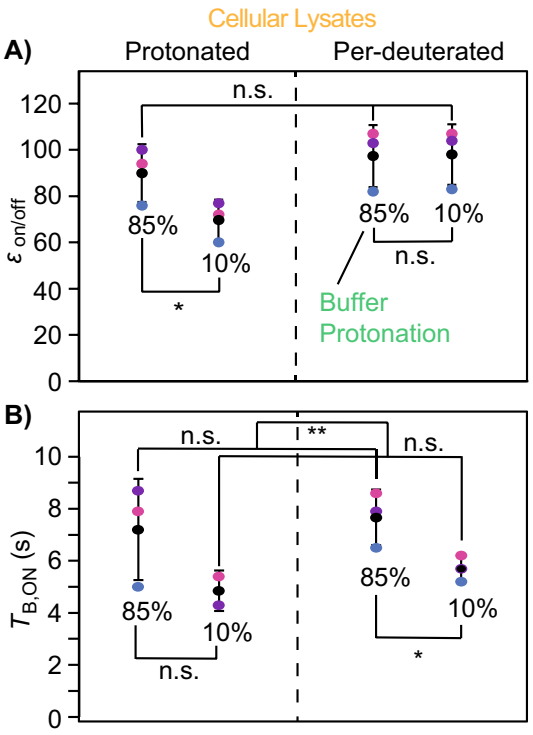

Fig. 2 DNP performance is maintained in protonated DNP matrix conditions for cellular lysate samples using AMUPol. DNP sample buffer protonation scheme is marked with 85% or 10%. DNP cellular lysate protonation scheme is marked with protonated (100%) or per-deuterated (30% proton content). Samples from the same data sets are indicated by color (pink, purple and blue). Average and standard deviations are shown in black. Black lines indicate results of paired student t-tests. **A** DNP enhancement ($\varepsilon_{on/off}$) of cellular lysate samples measured by the ratio of on/off microwaves signal of the ^{13}C–CP signal at the carbonyl. **B** Build-up time values derived from ^{1}H-saturation recovery experiments fit to a stretched exponential function at the carbonyl are dependent upon the protonation of the buffer. Samples contain 15% d_8-glycerol. Brackets indicate results of paired two-tailed homoscedastic student's t-tests (n.s. $p > 0.05$, * $p < 0.05$, ** $p < 0.01$)

right). This suggested that DNP enhancements when using AMUPol as the polarizing agent in lysate samples are not sensitive to the protonation level of the DNP sample buffer though overall DNP performance is improved through the shorter $T_{B,ON}$ values in protonated systems.

To determine if per-deuteration of the biological components of the cellular lysates improved DNP performance, we prepared DNP sample sets that contained fully protonated cellular lysates and compared the DNP enhancement and $T_{B,ON}$ with the per-deuterated lysates. We found that the DNP enhancement for samples of fully protonated lysates with 10% protonated DNP sample buffer were smaller than samples with all other combinations of protonation levels of the lysate and buffer by ~ 30% (Fig. 2A, Student's t-test, paired, $p < 0.05$, n = 3), although the lower intensity for the sample made with 10% protonated buffer and perdeuterated lysates was a trivial result of a larger off-signal in the presence of protonated lysates that results from higher overall protonation and a shorter $T_{B,ON}$. The absolute sensitivity of these experiments as assessed by the microwave on-signal intensities were similar regardless of the deuteration level of the lysate. We also found that samples with a proton content of 85%, rather than 10%, had longer $T_{B,ON}$ values (Fig. 2B, Student's t-test paired, $p < 0.001$, n = 6). This difference was not a result of differences in radical dispersion between protonated and deuterated sample because the β-factors were not affected by deuteration level (Student's t-test, paired, $p = 0.25$, n = 6, data not shown). However, when we probed for the uniformly isotopically enriched, fully protonated Sup35NM using ^{15}N-filtered experiments, we found that the $T_{B,ON}$ values were not sensitive to sample deuteration levels (Student's t-test, paired, $p = 0.49$, $n = 6$, Figure S3), therefore the deuteration level modestly affects the spectroscopy of the cellular milieu but does not alter the spectroscopy of the protein of interest. Taken together, we found that highly protonated environments have modest effects on the DNP performance of AMUPol in both glycerol/water matrices and matrices containing cellular lysates. This indicates that good DNP performance from AMUPol can be expected for per-deuterated as well as fully protonated biological systems.

Isotopically enriched proteins can be specifically detected at nanomolar concentrations in cellular milieu

The sensitivity enhancements that can be obtained for proteins diluted in biological milieu are sufficient to easily detect isotopes present at natural abundance in the sample. Thus, we calculated the expected selectivity ratio for a uniformly isotopically enriched protein diluted in yeast cellular lysates containing isotopes at their natural abundance. To do so, we determined the amount of ^{13}C labeled carbonyl carbons in the 30 kDa uniformly isotopically enriched protein of interest, Sup35NM, at a concentration of 25 µM and the amount of ^{13}C labeled carbonyl carbons present from natural abundance in the protein component of yeast lysates. The calculated amount of ^{13}C labeled carbonyl carbon in the uniformly isotopically labeled Sup35NM at 25 µM and the calculated amount of ^{13}C labeled carbonyl carbon in natural abundance yeast lysates were approximately equivalent when directly detecting ^{13}C (e.g., ^{13}C CP) (Fig. 3, dashed black line). Due to the lower natural abundance of ^{15}N, the calculated amount of ^{15}N labeled protein backbone nitrogen in the Sup35NM was two-fold larger than that of ^{15}N labeled protein backbone nitrogen in the yeast lysate (Groves et al. 1996; Frederick et al. 2015; Łabędź et al. 2017; Oftadeh et al. 2021). Thus, in directly detected ^{13}C or ^{15}N NMR experiments, the signals from natural abundance in the yeast lysate are predicted to account for half of the ^{13}C carbonyl signals and a third of the ^{15}N backbone signal.

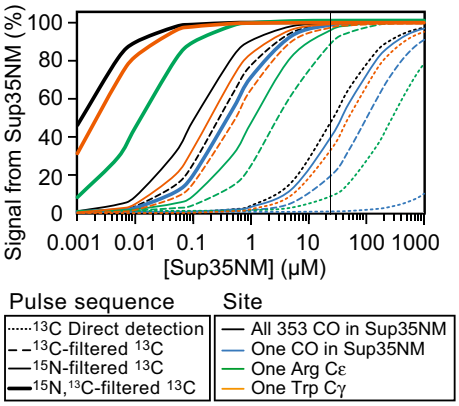

Fig. 3 Calculated specificity for the isotopically enriched protein of interest diluted in natural abundance cellular milieu depends upon the concentration of the protein of interest, the selectivity of the pulse sequence, and the degeneracy of the chemical shift of the site. The percent of the signal that is derived from isotopically enriched Sup35NM rather than from the natural molecules in the cellular milieu increases as the concentration of Sup35NM added to the sample increases. When Sup35NM is present at 25 μM (vertical line), the signal from all the carbonyl carbons in Sup35NM and from the cellular milieu is calculated to be of equal magnitude (dotted black line). Selection for sites with an adjacent isotopically labeled carbon (dashed lines) or nitrogen (solid lines) decreases the contribution from the cellular milieu by two orders of magnitude. Selection for a site through two adjacent isotopically labeled sites (thick lines) decreases the contribution from the cellular milieu by four orders of magnitude. All amino acids have at least one carbonyl moiety so specific detection of a single labeled CO site requires high concentrations and/or very selective pulse sequences (blue lines). Single sites in less abundant amino acids and/or in unique chemical moieties can be specifically detected at lower concentrations. About 5% of the amino acids in yeast are Arg (green) while only 1% are Trp (orange). With the use of highly selective pulse sequences these sites can be specifically detected (> 98%) at 100 nM or lower concentrations

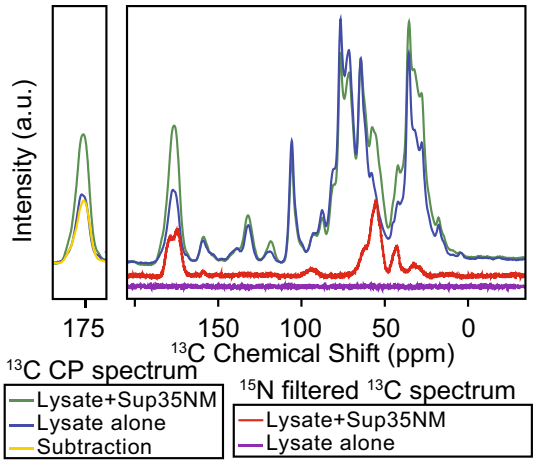

Fig. 4 The protein of interest and naturally abundant cellular lysates have predictable magnitudes of contribution to the spectrum. The ^{13}C spectra of natural abundance lysate alone (blue) has many signals while the ^{15}N filtered ^{13}C spectra has none (purple). The ^{13}C spectra of 25 μM of isotopically enriched Sup35NM diluted in natural abundance lysates (green) has many signals while the ^{15}N filtered ^{13}C spectra reports uniquely on the isotopically enriched Sup35NM (red). Subtraction of the blue spectrum from the green spectrum results in the yellow spectrum (left). All data were collected at 600 MHz with 395 GHz microwave irradiation at 104 K with a recycling delay of 7 s

We experimentally determined the selectivity ratio for a uniformly isotopically enriched Sup35NM at 25 μM diluted in lysates of yeast harboring the strong prion phenotype. To do so, we collected ^{13}C detected proton-carbon cross-polarization (^{13}C–CP) spectra (Pines et al. 1973) of lysates of yeasts grown on isotopically naturally abundant media in the presence and absence of 25 μM of isotopically-enriched Sup35NM (Fig. 4). Both spectra had peaks for carbonyl, aromatic, and aliphatic carbons, which are plentiful in proteins, and peaks for alcohol and ester carbons, which are plentiful in cell wall carbohydrates (~ 70–106 ppm). The protein peaks were more intense in the spectra of isotopically enriched Sup35NM diluted in cellular lysates (Fig. 4, green) than in the spectrum of lysates alone (Fig. 4, blue), while the cell wall carbohydrate peak intensities were similar. Subtraction of the spectrum of natural abundance lysate alone from the spectrum of Sup35NM diluted in natural abundance lysates removes the spectral contribution from lysates and the resulting spectrum should report only on the Sup35NM present in the sample. The intensity of the carbonyl peak in the subtracted spectrum (Fig. 4, yellow) was the same as the intensity of the carbonyl peak in the spectra of lysates alone (Fig. 4, blue), in line with the theoretical selectivity ratio of one to one. The theoretically-determined and the experimentally-determined selectivity ratios for 25 μM isotopically enriched protein diluted in natural abundance lysates agree.

Experiments that report only on sites that are near other NMR-active nuclei—something that is probable in the isotopically enriched protein (100% of sites) and improbable in the cellular lysates—increase the selectivity of the experiment for the protein of interest. Selective experiments increase the selectivity for the protein of interest albeit at the expense of some experimental sensitivity (Kehlet et al. 2004). Considering only the ^{13}C labeled carbonyl carbons that are directly bonded to another ^{13}C site, the calculated contribution from a 30 kDa protein to the total signal is one hundred times larger than the contribution from the yeast lysate and considering only the ^{13}C labeled carbonyl carbons that are directly bonded to another ^{15}N site, the calculated contribution from the uniformly isotopically enriched protein to the total signal is two hundred times larger than the contribution from the yeast lysate. We experimentally assessed the selectivity ratio for a uniformly isotopically enriched Sup35NM at 25 μM diluted in yeast lysates. To do so, we collected ^{15}N filtered ^{13}C detected spectra (TEDOR) (Jaroniec et al. 2002) of lysates of yeasts grown

on isotopically naturally abundant media in the presence and absence of 25 μM of isotopically-enriched Sup35NM (Fig. 4) (Pines et al. 1973). The spectrum of isotopically enriched Sup35NM diluted in cellular lysates had peaks for the carbonyl and Cα carbons, which are adjacent to the amide nitrogen in the protein backbone and, as expected, did not have peaks for aromatic and alcohol and ester carbons (~ 70–106 ppm). Likewise, as expected at this signal to noise level, no carbon signals were detected in spectrum of lysates alone (Fig. 4). Thus, using pulse sequences that select for adjacent isotopes, specific detection of uniformly isotopically enriched proteins in natural abundance yeast lysates at concentrations in the hundreds of nanomolar is theoretically possible (Fig. 3).

Specific detection of single protein sites in cellular milieu

The selectivity ratio for an isotopically enriched protein diluted in natural abundance lysates depends not only on the concentration of the protein but also the number of isotopically enriched sites in the protein of interest. Therefore, we determined the selectivity ratio in the limiting case where only single carbonyl carbon is uniformly isotopically enriched. Sup35NM has 253 amino acids and some of these amino acids have carbonyl carbons in the sidechain as well as the backbone so Sup35NM that is isotopically enriched only at a single site would have ~ 353 times fewer labeled sites so the contribution of a single labeled amino acid is ~ 353 times smaller. Thus, in a ^{13}C NMR experiment that is directly-detected, a protein harboring a single isotopically labeled amino acid must be present at 6.25 mM and, in an ^{15}N-filtered experiment, the protein must be present at 35 μM for the ^{13}C carbonyl signal from a single labeled site to account for half of the ^{13}C carbonyl signal (Fig. 3, blue). However, the carbonyl carbon site represents the most challenging case for detection of a single labeled amino acid in a protein because the amino acids in the protein and the cellular milieu have an average of ~ 1.25 carbonyl carbons and all carbonyl carbons fall within a relatively narrow range of chemical shifts. The selectivity ratios are better for sites and amino acids with distinct, rather than degenerate, chemical shifts. For example, arginine accounts for 5% of the amino acids in yeast and tryptophan accounts for 1% of the amino acids in yeast. Thus, detection of an arginine Cε site or a tryptophan Cγ site is 25- and 125- fold more selective, respectively, than detection of a carbonyl carbon because there are many fewer atoms in the sample with similar chemical shifts (Fig. 3, green, orange). Use of pulse sequences that select for three adjacent atoms, instead of two, will be 100- fold more selective. For the CO, which is the most degenerate site, selection for three adjacent atoms will enable specific detection of a single labeled CO site at low micromolar concentrations (Fig. 3, thick line). For a Trp site, selection for three adjacent atoms will enable specific detection for concentrations of tens of nanomolar in natural abundance cellular milieu. The selectivity ratio of uniformly isotopically enriched proteins diluted in natural abundance lysates depends upon both the concentration of the protein and number of isotopically enriched sites with degenerate chemical shifts. Thus, site-specific detection of single amino acid sites in a protein with distinct chemical shifts in cellular milieu for proteins at high nanomolar concentrations is theoretically possible.

Finally, isotopic depletion of the lysate background could potentially improve selectively for the isotopically enriched protein. We experimentally determined the selectivity ratio for a uniformly isotopically enriched Sup35NM at 25 μM diluted in lysates of yeast harboring the strong prion phenotype grown in isotopically depleted media. Because laboratory yeast strains are genetically altered to harbor nutritional defects, we grew yeast in complete synthetically-defined media (SD-CSM) which was made with ^{13}C-depleted glucose (0.01%) and ^{15}N-depleted ammonium sulfate (0.001%) as carbon and nitrogen sources but is supplemented with natural abundance amino acids and nutrients. We collected ^{13}C detected ^{13}C–CP spectra of lysates of yeasts grown on isotopically-depleted media in the presence and absence of 25 μM of uniformly isotopically-enriched Sup35NM (Figure S4A). The peak positions and relative intensities of the spectra of the isotopically depleted lysates alone were the same as those for natural abundance lysates alone but the total intensity of the isotopically-depleted lysates was half that of the natural abundance lysates (Figure S4B). Growth on isotopically depleted media resulted in a 50% reduction in the isotopic content of the lysates. This degree of depletion is in line with expectations because yeast will preferentially use the natural abundance amino acids present in the media. We next compared the spectra of isotopically depleted lysates in the presence and absence of Sup35NM and found that the signal intensities for the cell wall components in these spectra were similar (Figure S4A) while the signal intensities for proteins were four times more intense in the spectrum of the sample that contained Sup35NM. Subtraction of the spectrum of the isotopically-depleted lysates alone from the spectrum of Sup35NM in isotopically-depleted lysates removes the spectral contribution from lysates and the resulting spectrum reported only on the Sup35NM present in the sample (Figure S4A, orange). The intensity of the subtracted spectrum (Figure S4A, gold) is twice that of the depleted lysate alone (Figure S4A, light blue), in agreement with the degree of isotopic depletion of the lysates. Thus, growth of cells on isotopically-depleted nutritional sources decreased the signal contribution from the cellular background proportional to the degree of isotopic depletion. If the isotope content in the yeast lysates is reduced further,

which could be accomplished by growing prototrophic yeast on minimal media made with isotopically depleted carbon and nitrogen sources, specific detection of uniformly isotopically enriched proteins in isotopically depleted yeast lysates at concentrations in the low nanomolar range is theoretically possible (Costello et al. 2019). Thus, for samples with homogenously dispersed AMUPol and well-ordered protein sites, the concentration of proteins that can be specifically detected in cellular lysates far surpasses the practical limit of experimental sensitivity.

Finally, to assess the site-specific detection of single amino acid sites in a protein in cellular milieu, we collected two-dimensional carbon–nitrogen correlation spectra (zTEDOR) of 25 µM Sup35NM in yeast lysates. The DNP enhancement was 72 for this sample, which was made with fully protonated buffer and yeast lysates and cryoprotected with 15% glycerol. The signal to noise ratio for the carbonyl carbon peak was 115 after 23 h of acquisition time. The resolution of this spectrum enabled identification of amino acids with distinct ^{13}C–^{15}N chemical shifts (Fig. 5). Of the six amino acids with adjacent nitrogen-carbon pairs with chemical shifts that are distinguished by 10 ppm or more from the average for protein backbone chemical shifts, Sup35NM contains all but tryptophan (Fig. 5A) with 25 lysines, 23 glycines, 14 prolines, 2 arginines and 1 histidine. There were resolvable peaks in the spectra for the lysine Cε-Nζ, the glycine Cα-N, the proline Cα-N & Cδ–N, and the arginine Cδ-Nε (Fig. 5A). These peaks had signal to noise ratios that ranged from 150:1 for the lysine peak to 18:1 for the arginine peak (Table S1). Because peak intensities for different chemical moieties are not necessarily quantitative, we collected a 2D zTEDOR spectra of purified uniformly isotopically enriched Sup35NM that had been polymerized into the amyloid form using lysates from strong [*PSI*$^+$] cells as a template (Frederick et al. 2014). The relative ratios of the peak heights and SNR for lysine, glycine, proline and arginine are statistically indistinguishable for Sup35NM diluted into lysates and purified Sup35NM ($p > 0.42$, student's t-test, paired). Peaks for neither histidine, which is present in Sup35NM but likely has multiple protonation

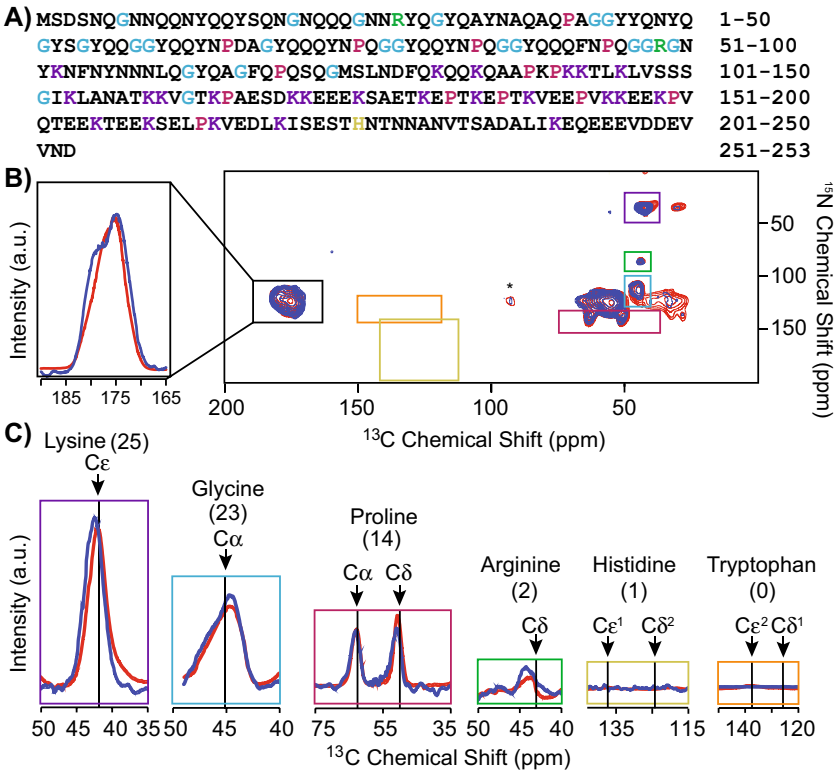

Fig. 5 Specific detection of isolated sites in Sup35NM in cellular milieu. **A** Protein sequence of Sup35NM. Lysines (purple), glycines (blue), prolines (pink), arginines (green) and histadine (yellow) are highlighted. **B** Two-dimensional ^{15}N-^{13}C correlation spectra (zTEDOR). Uniformly labeled Sup35NM in protonated, natural abundance strong [PSI$^+$] yeast lysate (blue) with 85% protonated buffer and 15% d_8-glycerol with 5 mM AMUPol, n = 1280, acquisition time = 23 h, $\varepsilon(on/off) = 72$. Purified amyloid fibers (red) with 10% protonation, 60% ^{13}C depleted d_8-glycerol with 10 mM AMUPol, n = 128, acquisition time = 2.5 h, $\varepsilon = 44$. Data were collected at 600 MHz with 12.5 kHz MAS at 104 K with a recycle delay of 4 s. Asterisks indicate spinning side bands. **C** Projections of regions of the zTEDOR for amino acids with unique chemical shifts for the lysate sample (colors, projected regions marked in (**B**) by boxes) overlayed on the purified fibril spectra (blue). The number of each amino acid in Sup35NM is indicated in paratheses. Arrows indicate the average chemical shifts from the BMRB for each site. Signal to noise ratios, integrated peak areas and centers are reported in Table S1

states under these conditions, nor tryptophan, which is not present in Sup35NM but is a component of the lysates, were not detected in either the two-dimensional spectra or the projections of the relevant regions (Fig. 5). Thus, site-specific detection of resolved amino acids sites for an isotopically enriched protein at low concentrations diluted in fully-protonated natural abundance cellular milieu is possible in tractable acquisition times.

To assess the influence of cellular milieu on the conformation of Sup35NM, we compared the spectra of Sup35NM that had been polymerized into the amyloid form using lysates from strong [*PSI*$^+$] cells as a template in the presence and absence of cellular milieu. In both samples, the average chemical shifts for the carbonyl, Cα and backbone nitrogen sites for all sites were consistent with β-sheet conformations, with larger shifts towards β-sheet chemical shift values for the Sup35NM assembled in cellular milieu (Table S1). The chemical shifts in both spectra for sites in the sidechains all fall within a standard deviation of the average value reported in the BMRB, but differ from each other; the center of the lysine Cε and arginine Cδ peaks were larger by 0.5 ppm when Sup35NM was polymerized in the presence, rather than the absence, of cellular milieu. The peak widths of the lysine, glycine and carbonyl carbon peaks were all broader for Sup35NM when polymerized in the presence rather than the absence of cellular milieu, reflecting a wider range of sampled conformations in the cellular milieu. Indeed, the carbonyl carbon peak for Sup35NM assembled in cellular milieu had a pronounced shoulder at chemical shift values consistent with the carbonyls in asparagine and glutamine sidechains, indicating that the sidechains are more ordered in the presence of cellular milieu than in its absence (Fig. 5). This indicates that the cellular milieu can, and does, influence protein conformations.

Discussion

The sensitivity enhancement from DNP NMR is theoretically sufficient to detect endogenous concentrations of isotopically-enriched proteins in biological environments. Yet, even with DNP, experiments are still sensitivity limited. To improve experimental sensitivity, we optimized sample composition and found that moderate concentrations of cryoprotectants improve absolute sensitivity without compromising enhancements and that per-deuteration does not improve DNP performance. The latter result indicates that good DNP performance can be expected in both per-deuterated and fully protonated cellular systems. Because at low target protein concentrations, the amount NMR-active isotopes in cellular biomass from natural abundance could be larger than that in the target protein, we experimentally validated theoretical calculations of the limit of specificity for an isotopically enriched protein in natural abundance cellular milieu. We establish that, using pulse sequences that are selective for adjacent NMR-active nuclei, it is possible that proteins can be specifically detected in cellular milieu at concentrations in the hundreds of nanomolar. In a fully protonated sample, cross peaks for isolated sites can be detected in under a day of acquisition time for the yeast prion protein, Sup35NM, when it is present at a concentration of 25 μM in concentrated yeast lysates. We found while there are no intensity differences in the spectra of purified Sup35NM and Sup35NM diluted in cellular lysates, which indicates that the cellular lysates did not contribute to the spectra, there were difference in the chemical shifts, which indicates that the cellular milieu can and does influence protein conformations.

Because cellular samples are sensitivity limited, we investigated the effect that the amount of cryoprotectant and level of deuteration had on DNP performance. Here we found that a cryoprotectant concentration of 15% (*v/v*) glycerol resulted in the highest absolute sensitivity for samples of proteins diluted in cellular milieu. Samples with higher concentrations of cryoprotectants had similar DNP enhancements but longer $T_{B,ON}$ and higher fill factors. While in this work, we limited our investigations to glycerol because isotopically depleted versions are commercially available, this is likely extendable to moderate concentrations of other cryoprotectants for cellular milieu (Xiao et al. 2021). For insoluble biomass, lowering the concentration of the cryoprotectant decreased the homogeneity of the dispersion of the polarization agent throughout the sample. This contrasts with reported results in mammalian cell systems (Ghosh et al. 2021, Xiao et al. 2021) as well as with results reported here with whole yeast lysates; the homogeneity of samples of mammalian cell derived milieu cryoprotected with 15% glycerol remained high as did whole lysates of yeast cells. Moreover, we found that although deuteration levels have a modest effect on the DNP properties of AMUPol, the deuteration level of the buffer and the cellular components did not alter the DNP properties of AMUPol in biological milieu. This indicates that the deuteration level doesn't significantly affect the DNP performance for these complex samples and, more generally, indicates that with modern radicals, per-deuteration may not be required at all for good DNP performance. Thus, here we find that in complex biological settings, reducing the amount of added cryoprotectant doubles the absolute sensitivity and that per-deuteration, which can alter the behavior of biological and cellular systems, is not a requirement for optimal DNP performance. Optimized sample compositions combined with modern polarization agents (Lund et al. 2020; Stevanato et al. 2020; Harrabi et al. 2022; Yao et al. 2022) will enable detection of proteins at concentrations in the high nanomolar range in tractable acquisition times.

The endogenous concentrations of many proteins range from hundreds of micromolar to tens of nanomolar. For samples that are homogenously doped with the polarization agent, the specificity limit for an isotopically enriched site in natural abundance cellular milieu depends upon the abundance of sites with chemical shifts that are degenerate with that of the isotopically-enriched site. Using pulse sequences that select for adjacent isotopically enriched sites, the theoretical specificity limit can range from hundreds of micromolar for a carbonyl site to single digit micromolar for sites with well-resolved chemical shifts. The specificity limit can be lowered by further isotopic depletion of the cellular background (Costello et al. 2019). However, the specificity limit can also be lowered by an additional two orders of magnitude by using more selective pulse sequences, such as those that incorporate selection steps that require not just two, but three, adjacent isotopically enriched sites (Pauli et al. 2001; Heise et al. 2005). Finally, while experimental specificity is an important consideration for samples that are homogenously doped with polarization agents where the analyte is diluted in an environment containing concentrated chemically similar natural abundance molecules, covalent attachment of the polarization to the target would effectively eliminate the specificity limit (Viennet et al. 2016; Lim et al. 2020). Likewise, experimental specificity is not a concern for molecules with chemical shifts that are distinct from those of the components of the cellular biomass (Schlagnitweit et al. 2019; Bertarello et al. 2022). Overall, with the currently available suite of DNP polarization agents, the specificity limit covers the range of endogenous concentrations for many proteins and is far lower than the practical sensitivity limit.

Here, we determined that by using selective pulse sequences, well-resolved single sites can potentially be specifically detected in yeast lysates when present at high nanomolar concentrations. Such calculations can be useful for other cellular systems. While not yet experimentally validated, the theoretical specificity limit for a single carbonyl site in mammalian cells is an order of magnitude lower than that for yeast because the protein density of the mammalian cells is lower than that of yeast (Milo 2013) and the relative abundance of the amino acids differs (Dietmair et al. 2012; Oftadeh et al. 2021). For the same reasons, the specificity limit in bacterial cells is expected to be an order of magnitude higher. Understanding the specificity limitations is useful for the design and interpretation of experiments of proteins in biological settings. For example, there are only two arginines in Sup35NM and the arginine Cδ–Nε correlations were detected with a SNR of 18:1 after 23 h of signal averaging for Sup35NM at 25 μM. However, for this protein system, the broader line widths under DNP conditions and chemical shift degeneracy precludes observation of single sites. Specific and segmental isotopic labeling effectively reduce chemical shift degeneracy of this protein (Frederick et al. 2017; Ghosh et al. 2018). Understanding the specificity limit defines the sample composition and choice of pulse sequences best suited to specifically detect unique sites for proteins at physiological concentrations from natural abundance isotopes present in the cellular milieu.

Prior work on the Sup35NM system indicated that a region that was intrinsically disordered in purified samples of Sup35NM fibrils underwent a large change in secondary structure when the protein was assembled into the amyloid form in cellular lysates (Frederick et al. 2015). In that work, the uniformly isotopically enriched Sup35NM at a concentration of 1 μM was diluted in isotopically depleted yeast lysates. The resulting increase in Sup35NM concentration in that sample was within range of endogenous levels since Sup35 is normally present at concentrations of 2.5 to 5 μM (Ghaemmaghami et al. 2003). In this work, the Sup35NM was present at a concentration of 25 μM, altering the stoichiometries of this protein with potential interactors by an order of magnitude, a perturbation that may potentially titrate out some interactions. Prior work reported on ^{13}C–^{13}C correlations, particularly those for well-resolved sites like the backbone CO–Cα, the lysine Cδ–Cε and the proline Cγ–Cδ. The present work reports on ^{13}C–^{15}N correlations. The sites that are most comparable to prior work are the backbone CO-N (which, in this work, includes contributions from the C'–N in the sidechains of Asn and Glu), the lysine Cε–Nζ, and the proline Cδ–N. The increase in β-sheet content for Sup35NM assembled in lysates relative to purified settings is maintained in both samples. However, while the chemical shifts of the sites in the lysine and proline sidechains differ for fibrils assembled in lysates and purified settings regardless of Sup35NM concentration, the magnitude of these differences, particularly for the proline Cδ, is smaller in the sample made with non-endogenous concentrations of Sup35NM. Because the changes in chemical shift are more modest for sites in the region of intrinsic disorder when Sup35NM is present at 25 μM, this suggests that the conformational rearrangement seen at lower concentrations is a result of specific interactions, rather than crowding. This further suggests that the relative stoichiometry of the protein of interest to the components of the cellular environment is an important experimental consideration, particularly for proteins that make specific interactions with cellular constituents.

Materials and methods

Sample preparation

Sup35NM was expressed and purified as described elsewhere (Serio et al. 1999). Uniformly-labeled ^{13}C ^{15}N Sup35NM samples were prepared by growing BL21(DES)-Rosetta

Escherichia coli in the presence of M9 media with 2 g L^{-1} D-glucose $^{1}H,^{13}C_6$ and 1 g L^{-1} of ^{15}N ammonium chloride (Cambridge Isotope Labs, Cambridge, MA). Purified, lysate-templated NM fibrils samples for the purified fiber sample were prepared as described elsewhere (Frederick et al. 2014; 2015), except that 5 mM AMUPol was used as the polarization agent (Sauvée et al. 2013).

Cell lysate samples for DNP

Cell lysate samples were prepared as previously described. (Frederick et al. 2015; Costello et al. 2019), with minor modifications. Briefly, phenotypically strong [PSI^{+}] yeast were grown in a 50 mL culture volume at 30 °C to mid-log phase in SD-CSM media made with protonated carbon sources and either 100% H_2O or 100% D_2O. Because we use protonated carbon sources, the final deuteration level for the lysates was 70% as determined by solution state NMR, as expected (Leiting et al. 1998). Isotopically depleted yeast lysates were made from yeast grown on SD-CSM made with yeast nitril base without amino acids and without ammonium sulfate (BD Scientific) supplemented by ^{13}C depleted D-Glucose (99.9% Cambridge Isotopes) and ^{15}N depleted ammonium sulfate (Sigma). Cells were collected by centrifugation (5 min, 4000×*g*) and washed once with water or D_2O, depending upon final level of sample perdeuteration. Pellets were suspended in 200 µL of lysis buffer (50 mM Tris–HCl pH 7.4, 200 mM NaCl, 2 mM TCEP, 5% d_8-^{13}C depleted glycerol, 1 mM EDTA, 5 ug/mL of aprotinin and leupeptin and 100 µg/mL Roche protease inhibitor cocktail. Deuteration of the lysis buffer was adjusted as required.) Cells were lysed by bead beating with 500 µm acid washed glass beads for 8 min at 4 °C. After bead beating, the bottom of the Eppendorf tube was punctured with a 22G needle and the entire lysate mixture was transferred to a new tube. Purified denatured $^{13}C^{15}N$-labeled Sup35NM was diluted at least 150-fold out of 6 M GdHCl to a final concentration of 5 µM and the mixture was allowed to polymerize, quiescent, at 4 °C for 24 to 48 h. The insoluble portion of the sample was collected by centrifugation at 20,000×*g* for 1 h at 4 °C and removal of the supernatant. The ~ 30 µL pellet was resuspended in various amounts of 100% d_8-^{13}C depleted glycerol and transferred to a 3.2 mm sapphire rotor. The final radical concentration was 5 mM of AMUPol (Sauvée et al. 2013). The isotopically depleted cell lysate samples were made analogously, except that yeast cells were grown in SD-CSM media made with 2% (*w/v*) protonated ^{13}C-depleted glucose (99.9% ^{12}C, Cambridge Isotope Labs) as the carbon source. Whole yeast lysate samples were made by growing the w303 strain of *S. cerevisiae* that were corrected for auxotrophies at all loci were cultured in synthetic defined yeast media (SD-min) made with 2% (*w/v*) D-glucose-$^{13}C_6$ (Sigma), 0.225% (*w/v*) $^{15}NH_4Cl$ (Sigma), and 0.17% nitrogen base without ammonium sulfate and amino acids (Difco). Cells were grown at 30 °C to mid log phase, collected by centrifugation and washed twice with D_2O. Cells were buffered with a phosphate buffer (10 mM potassium phosphate, 100 mM NaCl, pH = 6.0) and suspended in d_8-^{12}C-glycerol/D_2O/H_2O for a final composition of 15:75:10 with 5 mM AMUPol. The cells from the suspension were pelleted into a 3.2 mm rotor and lysed freeze-thawing the yeast cells in the rotor three-times. The yeast lysate was stored at -80 °C until data collection.

Immunohistochemistry

Cell lysate samples were made as described above. Sup35NM was visualized using an antibody raised against residue 125–253 of the protein (GenScript). Cell lysates were fractionated by SDS-PAGE, transferred to nitrocellulose and probed with the anti-Sup35NM antibodies. Lysate samples were denatured by incubation at 95 °C for 10 min in the presence of 2% SDS before fractionation to denature amyloid aggregates. Secondary antibodies were coupled to horseradish peroxidase. Blots were visualized by a standard ECL analysis.

Spectroscopy

Dynamic nuclear polarization magic angle spinning nuclear magnetic resonance (DNP MAS NMR) experiments were performed on 600 MHz Bruker Ascend DNP NMR spectrometers with 7.2 T Cryogen-free gyrotron magnet (Bruker), equipped with a ^{1}H, ^{13}C, ^{15}N triple-resonance, 3.2 mm low temperature (LT) DNP MAS NMR Bruker probe (600 MHz). The sample temperature was 104 K, at MAS frequency of 12 kHz. The DNP enhancements on these instrumentation set-ups for a standard sample of 1.5 mg of uniformly ^{13}C, ^{15}N labeled proline (Isotech) suspended in 25 mg of 60:30:10 d_8-glycerol:D_2O:H_2O containing 10 mM AMUPol varied between 80 and 140. The DNP enhancements that were measured close in time on the same spectrometer were compared quantitively within the set and qualitatively between sets.

In ^{13}C cross-polarization (CP) MAS experiments, the ^{13}C radio frequency (RF) amplitude was linearly swept from 75 to 37.5 kHz with an average of 56.25 kHz. ^{1}H RF amplitude was kept at 68 ~ 72 kHz for CP, 83 kHz for 90 degree pulse, and 85 kHz for ^{1}H TPPM decoupling with phase alternation of ± 15° during acquisition of ^{13}C signal. The DNP enhancements were determined by comparing 1D ^{13}C CP spectra collected with and without microwaves irradiation. For $T_{B,on}$ measurements, recycle delays ranged from 0.1 s to 300 s. To determine the $T_{B,on}$, the dependence of the recycle delay on both ^{13}C peak intensity or volume was fit to the equation $I_t = I_0 \times [1 - e^{-\left(\frac{t}{TBon}\right)}]$. For ^{13}C-^{15}N 1D and 2D

correlations, a 1.92 ms TEDOR sequence was applied with ^{13}C and ^{15}N pulse trains at 55.5 kHz and 41.7 kHz, respectively. A total of 64 complex t_1 points with an increment of 80 µs were recorded. Data were processed using NMRPipe software and analyzed in Sparky.

Supplementary Information The online version contains supplementary material available at https://doi.org/10.1007/s10858-024-00436-9.

Author contributions KKF and WNC wrote the main manuscript text. WNC prepared figures 1, 2, 4 & 5. YX prepared figure 3. FM-V and JK performed experiments. All authors reviewed the manuscript.

Funding W.N.C. was supported by a graduate research fellowship from the NSF and NIH MB T32 GM008297. This work was supported by grants from the National Science Foundation [1751174]; the Welch Foundation [1-1923-20200401]; NIH R01NS134921; the Lupe Murchison Foundation, and the Kinship Foundation (Searle Scholars Program) to K.K.F. The National High Magnetic Field Laboratory (NHMFL) is supported by the NSF Division of Materials Research (DMR1644779 and DMR-2128556) and by the State of Florida. The 14.1T DNP system at NHMFL is supported by the National Institutes of Health Grant NIH P41 GM122698 and RM1 GM148766.

Declarations

Competing interest The authors declare no competing interests.

References

Albert BJ, Gao C, Sesti EL, Saliba EP, Alaniva N, Scott FJ, Sigurdsson ST, Barnes AB (2018) Dynamic nuclear polarization nuclear magnetic resonance in human cells using fluorescent polarizing agents. Biochemistry 57(31):4741–4746

Allen KD, Wegrzyn RD, Chernova TA, Müller S, Newnam GP, Winslett PA, Wittich KB, Wilkinson KD, Chernoff YO (2005) Hsp70 chaperones as modulators of prion life cycle: novel effects of Ssa and Ssb on the Saccharomyces cerevisiae prion [PSI+]. Genetics 169(3):1227–1242

Bajaj VS, Farrar CT, Hornstein MK, Mastovsky I, Vieregg J, Bryant J, Elena B, Kreischer KE, Temkin RJ, Griffin RG (2003) Dynamic nuclear polarization at 9T using a novel 250GHz gyrotron microwave source. J Magn Reson 160(2):85–90

Bajaj VS, Hornstein MK, Kreischer KE, Sirigiri JR, Woskov PP, Mak-Jurkauskas ML, Herzfeld J, Temkin RJ, Griffin RG (2007) 250GHz CW gyrotron oscillator for dynamic nuclear polarization in biological solid state NMR. J Magn Reson 189(2):251–279

Banci L, Barbieri L, Bertini I, Luchinat E, Secci E, Zhao Y, Aricescu AR (2013) Atomic-resolution monitoring of protein maturation in live human cells by NMR. Nat Chem Biol 9(5):297–299

Berruyer P, Björgvinsdóttir S, Bertarello A, Stevanato G, Rao Y, Karthikeyan G, Casano G, Ouari O, Lelli M, Reiter C, Engelke F, Emsley L (2020) Dynamic nuclear polarization enhancement of 200 at 21.15 T enabled by 65 kHz magic angle spinning. J Phys Chem Lett 11(19):8386–8391

Bertarello A, Berruyer P, Artelsmair M, Elmore CS, Heydarkhan-Hagvall S, Schade M, Chiarparin E, Schantz S, Emsley L (2022) In-cell quantification of drugs by magic-angle spinning dynamic nuclear polarization NMR. J Am Chem Soc 144(15):6734–6741

Burmann BM, Gerez JA, Matečko-Burmann I, Campioni S, Kumari P, Ghosh D, Mazur A, Aspholm EE, Šulskis D, Wawrzyniuk M (2020) Regulation of α-synuclein by chaperones in mammalian cells. Nature 577(7788):127–132

Costello WN, Xiao Y, Frederick KK (2019) DNP-assisted NMR investigation of proteins at endogenous levels in cellular milieu. Methods Enzymol 615:373–406

Dietmair S, Hodson MP, Quek LE, Timmins NE, Gray P, Nielsen LK (2012) A multi-omics analysis of recombinant protein production in Hek293 cells. PLoS ONE 7(8):e43394

Elathram N, Ackermann BE, Debelouchina GT (2022) DNP-enhanced solid-state NMR spectroscopy of chromatin polymers. J Magn Reson Open 10–11:100057

Frederick KK, Debelouchina GT, Kayatekin C, Dorminy T, Jacavone AC, Griffin RG, Lindquist S (2014) Distinct prion strains are defined by amyloid core structure and chaperone binding site dynamics. Chem Biol 21(2):295–305

Frederick KK, Michaelis VK, Corzilius B, Ong T-C, Jacavone AC, Griffin RG, Lindquist S (2015) Sensitivity-enhanced NMR reveals alterations in protein structure by cellular milieus. Cell 163(3):620–628

Frederick KK, Michaelis VK, Caporini MA, Andreas LB, Debelouchina GT, Griffin RG, Lindquist S (2017) Combining DNP NMR with segmental and specific labeling to study a yeast prion protein strain that is not parallel in-register. Proc Natl Acad Sci USA 114(14):3642–3647

Freedberg DI, Selenko P (2014) Live cell NMR. Annu Rev Biophys 43:171–192

Ghaemmaghami S, Huh WK, Bower K, Howson RW, Belle A, Dephoure N, O'Shea EK, Weissman JS (2003) Global analysis of protein expression in yeast. Nature 425(6959):737–741

Ghosh R, Dong J, Wall J, Frederick KK (2018) Amyloid fibrils embodying distinctive yeast prion phenotypes exhibit diverse morphologies. FEMS Yeast Res. https://doi.org/10.1093/femsyr/foy059

Ghosh R, Xiao Y, Kragelj J, Frederick KK (2021) In-cell sensitivity-enhanced NMR of intact viable mammalian cells. J Am Chem Soc 143(44):18454–18466

Groves JD, Falson P, le Maire M, Tanner MJ (1996) Functional cell surface expression of the anion transport domain of human red cell band 3 (AE1) in the yeast *Saccharomyces cerevisiae*. Proc Natl Acad Sci 93(22):12245–12250

Gupta S, Tycko R (2018) Segmental isotopic labeling of HIV-1 capsid protein assemblies for solid state NMR. J Biomol NMR 70(2):103–114

Gupta R, Lu M, Hou G, Caporini MA, Rosay M, Maas W, Struppe J, Suiter C, Ahn J, Byeon I-JL (2016) Dynamic nuclear polarization enhanced MAS NMR spectroscopy for structural analysis of HIV-1 protein assemblies. J Phys Chem B 120(2):329–339

Hall DA, Maus DC, Gerfen GJ, Inati SJ, Becerra LR, Dahlquist FW, Griffin RG (1997) Polarization-enhanced NMR spectroscopy of biomolecules in frozen solution. Science 276(5314):930–932

Harrabi R, Halbritter T, Aussenac F, Dakhlaoui O, van Tol J, Damodaran KK, Lee D, Paul S, Hediger S, Mentink-Vigier F, Sigurdsson ST, De Paepe G (2022) Highly efficient polarizing agents for MAS-DNP of proton-dense molecular solids. Angew Chem Int Ed Engl 61(12):e202114103

Heiliger J, Matzel T, Cetiner EC, Schwalbe H, Kuenze G, Corzilius B (2020) Site-specific dynamic nuclear polarization in a Gd(III)-labeled protein. Phys Chem Chem Phys 22(44):25455–25466

Heise H, Seidel K, Etzkorn M, Becker S, Baldus M (2005) 3D NMR spectroscopy for resonance assignment and structure elucidation of proteins under MAS: novel pulse schemes and sensitivity considerations. J Magn Reson 173(1):64–74

Helsen CW, Glover JR (2012) Insight into molecular basis of curing of [PSI+] prion by overexpression of 104-kDa heat shock protein (Hsp104). J Biol Chem 287(1):542–556

Inaba A, Andersson O (2007) Multiple glass transitions and two step crystallization for the binary system of water and glycerol. Thermochim Acta 461(1):44–49

Inomata K, Ohno A, Tochio H, Isogai S, Tenno T, Nakase I, Takeuchi T, Futaki S, Ito Y, Hiroaki H (2009) High-resolution multi-dimensional NMR spectroscopy of proteins in human cells. Nature 458(7234):106–109

Jaroniec CP, Filip C, Griffin RG (2002) 3D TEDOR NMR experiments for the simultaneous measurement of multiple carbon− nitrogen distances in uniformly 13C, 15N-labeled solids. J Am Chem Soc 124(36):10728–10742

Kang X, Kirui A, Dickwella Widanage MC, Mentink-Vigier F, Cosgrove DJ, Wang T (2019) Lignin-polysaccharide interactions in plant secondary cell walls revealed by solid-state NMR. Nat Commun 10(1):347

Kaplan M, Narasimhan S, de Heus C, Mance D, van Doorn S, Houben K, Popov-Čeleketić D, Damman R, Katrukha EA, Jain P (2016) EGFR dynamics change during activation in native membranes as revealed by NMR. Cell 167(5):1241-1251. e1211

Kaplan M, Narasimhan S, de Heus C, Mance D, van Doorn S, Houben K, Popov-Celeketic D, Damman R, Katrukha EA, Jain P, Geerts WJC, Heck AJR, Folkers GE, Kapitein LC, Lemeer S, van Bergen En PMP, Henegouwen and M. Baldus, (2016) EGFR dynamics change during activation in native membranes as revealed by NMR. Cell 167(5):1241-1251 e1211

Kehlet CT, Sivertsen AC, Bjerring M, Reiss TO, Khaneja N, Glaser SJ, Nielsen NC (2004) Improving solid-state NMR dipolar recoupling by optimal control. J Am Chem Soc 126(33):10202–10203

Kiktev DA, Patterson JC, Müller S, Bariar B, Pan T, Chernoff YO (2012) Regulation of chaperone effects on a yeast prion by cochaperone Sgt2. Mol Cell Biol 32(24):4960–4970

Łabędź B, Wańczyk A, Rajfur Z (2017) Precise mass determination of single cell with cantilever-based microbiosensor system. PLoS ONE 12(11):e0188388

Lane LB (1925) Freezing points of glycerol and its aqueous solutions. Ind Eng Chem 17(9):924–924

Leiting B, Marsilio F, O'Connell JF (1998) Predictable deuteration of recombinant proteins expressed in *Escherichia coli*. Anal Biochem 265(2):351–355

Liao SY, Lee M, Wang T, Sergeyev IV, Hong M (2016) Efficient DNP NMR of membrane proteins: sample preparation protocols, sensitivity, and radical location. J Biomol NMR 64(3):223–237

Lim BJ, Ackermann BE, Debelouchina GT (2020) Targetable tetrazine-based dynamic nuclear polarization agents for biological systems. ChemBioChem 21(9):1315–1319

Lund A, Casano G, Menzildjian G, Kaushik M, Stevanato G, Yulikov M, Jabbour R, Wisser D, Renom-Carrasco M, Thieuleux C, Bernada F, Karoui H, Siri D, Rosay M, Sergeyev IV, Gajan D, Lelli M, Emsley L, Ouari O, Lesage A (2020) TinyPols: a family of water-soluble binitroxides tailored for dynamic nuclear polarization enhanced NMR spectroscopy at 18.8 and 21.1 T. Chem Sci 11(10):2810–2818

Märker K, Paul S, Fernández-de-Alba C, Lee D, Mouesca J-M, Hediger S, De Paëpe G (2017) Welcoming natural isotopic abundance in solid-state NMR: probing π-stacking and supramolecular structure of organic nanoassemblies using DNP. Chem Sci 8(2):974–987

Masison DC, Kirkland PA, Sharma D (2009) Influence of Hsp70s and their regulators on yeast prion propagation. Prion 3(2):65–73

Mentink-Vigier F, Vega S, De Paëpe G (2017) Fast and accurate MAS–DNP simulations of large spin ensembles. Phys Chem Chem Phys 19(5):3506–3522

Milo R (2013) What is the total number of protein molecules per cell volume? A call to rethink some published values. BioEssays 35(12):1050–1055

Misra PM (1967) The effects of deuterium on living organisms. Curr Sci 36(17):447–453

Mollica G, Dekhil M, Ziarelli F, Thureau P, Viel S (2015) Quantitative structural constraints for organic powders at natural isotopic abundance using dynamic nuclear polarization solid-state NMR spectroscopy. Angew Chem Int Ed Engl 54(20):6028–6031

Narasimhan S, Scherpe S, Lucini Paioni A, van der Zwan J, Folkers GE, Ovaa H, Baldus M (2019a) DNP-supported solid-state NMR spectroscopy of proteins inside mammalian cells. Angew Chem Int Ed Engl 58(37):12969–12973

Narasimhan S, Scherpe S, Lucini Paioni A, Van Der Zwan J, Folkers GE, Ovaa H, Baldus M (2019b) DNP-supported solid-state NMR spectroscopy of proteins inside mammalian cells. Angew Chem 131(37):13103–13107

Nollen EA, Morimoto RI (2002) Chaperoning signaling pathways: molecular chaperones as stress-sensingheat shock'proteins. J Cell Sci 115(14):2809–2816

Oftadeh O, Salvy P, Masid M, Curvat M, Miskovic L, Hatzimanikatis V (2021) A genome-scale metabolic model of *Saccharomyces cerevisiae* that integrates expression constraints and reaction thermodynamics. Nat Commun 12(1):4790

Pauli J, Baldus M, van Rossum B, de Groot H, Oschkinat H (2001) Backbone and side-chain 13C and 15N signal assignments of the alpha-spectrin SH3 domain by magic angle spinning solid-state NMR at 17.6 Tesla. ChemBioChem 2(4):272–281

Pines A, Gibby MG, Waugh JS (1973) Proton-enhanced NMR of dilute spins in solids. J Chem Phys 59(2):569–590

Pinon AC, Schlagnitweit J, Berruyer P, Rossini AJ, Lelli M, Socie E, Tang M, Pham T, Lesage A, Schantz S, Emsley L (2017) Measuring nano-to microstructures from relayed dynamic nuclear polarization NMR. J Phys Chem C 121(29):15993–16005

Qiang W, Yau W-M, Lu J-X, Collinge J, Tycko R (2017) Structural variation in amyloid-β fibrils from Alzheimer's disease clinical subtypes. Nature 541(7636):217

Rankin AGM, Trebosc J, Pourpoint F, Amoureux JP, Lafon O (2019) Recent developments in MAS DNP-NMR of materials. Solid State Nucl Magn Reson 101:116–143

Renault M, Tommassen-van Boxtel R, Bos MP, Post JA, Tommassen J, Baldus M (2012) Cellular solid-state nuclear magnetic resonance spectroscopy. Proc Natl Acad Sci 109(13):4863–4868

Rosay M (2001) Sensitivity-enhanced nuclear magnetic resonance of biological solids. Ph.D., Massachusetts Institute of Technology

Rosay M, Zeri AC, Astrof NS, Opella SJ, Herzfeld J, Griffin RG (2001) Sensitivity-enhanced NMR of biological solids: dynamic nuclear polarization of Y21M fd bacteriophage and purple membrane. J Am Chem Soc 123(5):1010–1011

Rosay M, Lansing JC, Haddad KC, Bachovchin WW, Herzfeld J, Temkin RJ, Griffin RG (2003) High-frequency dynamic nuclear polarization in MAS spectra of membrane and soluble proteins. J Am Chem Soc 125(45):13626–13627

Sakakibara D, Sasaki A, Ikeya T, Hamatsu J, Hanashima T, Mishima M, Yoshimasu M, Hayashi N, Mikawa T, Wälchli M (2009) Protein structure determination in living cells by in-cell NMR spectroscopy. Nature 458(7234):102–105

Sauvée C, Rosay M, Casano G, Aussenac F, Weber RT, Ouari O, Tordo P (2013) Highly efficient, water-soluble polarizing agents for dynamic nuclear polarization at high frequency. Angew Chem 125(41):11058–11061

Sauvee C, Rosay M, Casano G, Aussenac F, Weber RT, Ouari O, Tordo P (2013) Highly efficient, water-soluble polarizing agents for dynamic nuclear polarization at high frequency. Angew Chem Int Ed Engl 52(41):10858–10861

Scherpelz KP, Wang S, Pytel P, Madhurapantula RS, Srivastava AK, Sachleben JR, Orgel J, Ishii Y, Meredith SC (2021) Atomic-level differences between brain parenchymal- and cerebrovascular-seeded Aβ fibrils. Sci Rep 11(1):247

Schlagnitweit J, Sandoz SF, Jaworski A, Guzzetti I, Aussenac F, Carbajo RJ, Chiarparin E, Pell AJ, Petzold K (2019) Observing an

antisense drug complex in intact human cells by in-cell NMR. bioRxiv 589812
Schubeis T, Luhrs T, Ritter C (2015) Unambiguous assignment of short- and long-range structural restraints by solid-state NMR spectroscopy with segmental isotope labeling. ChemBioChem 16(1):51–54
Selenko P, Serber Z, Gadea B, Ruderman J, Wagner G (2006) Quantitative NMR analysis of the protein G B1 domain in Xenopus laevis egg extracts and intact oocytes. Proc Natl Acad Sci 103(32):11904–11909
Serio TR, Cashikar AG, Moslehi JJ, Kowal AS, Lindquist SL (1999) Yeast prion [psi +] and its determinant, Sup35p Methods. Enzymol 309:649–673
Song C, Hu KN, Joo CG, Swager TM, Griffin RG (2006) TOTAPOL: a biradical polarizing agent for dynamic nuclear polarization experiments in aqueous media. J Am Chem Soc 128(35):11385–11390
Stevanato G, Casano G, Kubicki DJ, Rao Y, Esteban Hofer L, Menzildjian G, Karoui H, Siri D, Cordova M, Yulikov M, Jeschke G, Lelli M, Lesage A, Ouari O, Emsley L (2020) Open and closed radicals: local geometry around unpaired electrons governs magic-angle spinning dynamic nuclear polarization performance. J Am Chem Soc 142(39):16587–16599
Takahashi H, Lee D, Dubois L, Bardet M, Hediger S, De Paëpe G (2012) Rapid natural-abundance 2D 13C–13C correlation spectroscopy using dynamic nuclear polarization enhanced solid-state NMR and matrix-free sample preparation. Angew Chem Int Ed 51(47):11766–11769
Theillet F-X, Rose HM, Liokatis S, Binolfi A, Thongwichian R, Stuiver M, Selenko P (2013) Site-specific NMR mapping and time-resolved monitoring of serine and threonine phosphorylation in reconstituted kinase reactions and mammalian cell extracts. Nat Protoc 8(7):1416
Tran NT, Mentink-Vigier F, Long JR (2020) Dynamic nuclear polarization of biomembrane assemblies. Biomolecules 10(9):1246
van der Wel PC, Hu KN, Lewandowski J, Griffin RG (2006) Dynamic nuclear polarization of amyloidogenic peptide nanocrystals: GNNQQNY, a core segment of the yeast prion protein Sup35p. J Am Chem Soc 128(33):10840–10846
van der Zwan KP, Riedel W, Aussenac F, Reiter C, Kreger K, Schmidt H-W, Risse T, Gutmann T, Senker J (2021) 19F MAS DNP for probing molecules in nanomolar concentrations: direct polarization as key for solid-state NMR spectra without solvent and matrix signals. J Phy Chem C 125(13):7287–7296
Viennet T, Viegas A, Kuepper A, Arens S, Gelev V, Petrov O, Grossmann TN, Heise H, Etzkorn M (2016) Selective protein hyperpolarization in cell lysates using targeted dynamic nuclear polarization. Angew Chem Int Ed Engl 55(36):10746–10750
Wang M, Weiss M, Simonovic M, Haertinger G, Schrimpf SP, Hengartner MO, von Mering C (2012) PaxDb, a database of protein abundance averages across all three domains of life. Mol Cell Proteom 11(8):492–500
Xiao Y, Ghosh R, Frederick KK (2021) In-cell NMR of intact mammalian cells preserved with the cryoprotectants DMSO and glycerol have similar DNP performance. Front Mol Biosci 8:789478
Yao R, Beriashvili D, Zhang W, Li S, Safeer A, Gurinov A, Rockenbauer A, Yang Y, Song Y, Baldus M, Liu Y (2022) Highly bioresistant, hydrophilic and rigidly linked trityl-nitroxide biradicals for cellular high-field dynamic nuclear polarization. Chem Sci 13(47):14157–14164
Zhai W, Lucini Paioni A, Cai X, Narasimhan S, Medeiros-Silva J, Zhang W, Rockenbauer A, Weingarth M, Song Y, Baldus M, Liu Y (2020) Postmodification via thiol-click chemistry yields hydrophilic trityl-nitroxide biradicals for biomolecular high-field dynamic nuclear polarization. J Phys Chem B 124(41):9047–9060